Iranian Journal of Materials Forming 8 (4) (2021) 15-25

Online ISSN: 2383-0042

IJMF

Iranian Journal of Materials Forming

Journal Homepage: http://ijmf.shirazu.ac.ir

Research Article

Study of Texture Weakening of Commercially Pure Copper Processed by Multiple Compressions in a Channel Die

Y. Lagzian and A. Rezaee-Bazzaz*

Department of Metallurgy and Materials Engineering, Faculty of Engineering, Ferdowsi University of Mashhad, Mashhad, Iran

ARTICLE INFO

Article history:

Received 9 July 2021
Reviewed 9 August 2021
Revised 17 August 2021
Accepted 10 September 2021

Keywords:

Severe plastic deformation
Anisotropy
Texture estimation

ABSTRACT

Texture evolution of commercially pure copper processed by multiple compressions in a channel die was investigated and interpreted by the use of continuity equation for the crystallographic orientation distribution function (ODF), which is considered as a kind of conservation law in the crystal orientation (Euler angle) space. The specimen has been subjected to multiple compressions in a channel die up to six passes, and its bulk texture after even passes of the process were measured by x-ray diffraction. Based on these experiments, it was found that during the multiple compressions in a channel die, Beta fiber strengthens at the beginning of the process and then weakens. The Cube component is observed in the texture of processed specimens, while Goss component is missing. Calculation of the texture index shows that the overall texture strength decreases during multiple compressions in a channel die. Deformation of each pass during the process is assumed to be analogous to that of flat rolling. After each pass of the process, the sample is rotated around two mutually perpendicular directions. The ODF of the processed sample during each pass of compression was predicted analytically as a function of the initial ODF and crystallographic rotation speed in the Euler angle space. Based on the predicted analytical function of ODF, the locations of the stable texture components and the evolution of texture can be estimated. After each pass of the process, as mentioned above, the specimen is rotated, therefore, the texture of the specimen with respect to this new sample frame should be considered as the initial texture for the subsequent pass of the process. Using the analytical function of ODF during each pass, texture evolution and stable texture components can be estimated during this new pass. Following the aforementioned stages, texture evolution during multiple compressions in a channel die was predicted, and a good agreement with experimentally determined texture evolution was obtained.

1. Introduction

Severe plastic deformation methods which can be used for the production of ultra-fine grained metals draw considerable attention [1, 2] due to extraordinary properties of materials processed by these methods, like, simultaneously enhanced strength and high ductility, relatively high conductivity and/or high strain rate superplasticity [3].

A number of severe plastic deformation techniques, such as Equal Channel Angular Pressing (ECAP) [4, 5],

* Corresponding author
E-mail address: bazaz-r@um.ac.ir (A. Rezaee-Bazzaz)
https://doi.org/10.22099/ijmf.2021.41140.1187

Accumulative Roll-Bonding (ARB) [6], Multi-Directional Forging (MDF) [7], and Cyclic Extrusion and Compression (CEC) [8] have been developed and utilized for the production of ultra-fine grained metals. Among these techniques, multi-directional forging is conceptually very simple. During MDF, the specimen undergoes uniaxial compression along three orthogonal axes, but after each pressing, the lateral sides of the sample are barreled. Therefore, these bulged surfaces need to be grinded to preserve the original shape of the sample and continue the process along a different axis. The necessity of grinding after every pass can be reduced by the use of a channel die, usually used to simulate plane strain rolling [9].

Microstructural evolution during MDF has been investigated in many research works and it has been shown that this technique is capable of producing ultra-fine grained metals [10-16]. Texture evolution of Al-3Mg-Sc(Zn) alloy during tri-axial forging was studied and it has been reported that a strong texture is produced at high temperatures while texture weakening occurs at lower ones [14]. Texture evolution of AISI 1016 steel subjected to six passes of warm MDF was investigated and occurrence of texture weakening was observed [15]. It has also been shown that texture weakening occurs at relatively low temperatures in magnesium alloys processed by MDF [10, 11, 13]. Texture weakening during MDF is thus common, regardless of the crystal structure of processed metals.

It has been proposed that with the help of the principle of conservation, applied to crystallographic orientation distribution function (ODF), a relationship for the prediction of deformation texture is derived. In this relationship, the rotation field in the crystal orientation (Euler angle) space is considered as the main parameter which completely describes the texture evolution [17, 18]. The equation obtained by the use of the conservation law for the change of ODF during deformation was used for prediction of ideal orientations during flat rolling of FCC polycrystals and the formation of Alpha and Beta fibers were predicted, and it was shown that boundary conditions affect the composition of Beta fiber and the flow velocity of orientations towards and along Alpha and Beta fibers [19]. The development of rolling textures of BCC polycrystals in low and extra low-carbon steels has also been investigated using the conservation law, and it has been found that the operation of preferred deformation modes is orientation-dependent [20]. The principle of conservation has also been utilized for the stability of texture analysis of IF steel during asymmetric rolling and displacement of ND fiber in the Euler angle space reported [21].

Reviewing literature shows that there have been few attempts for investigating texture evolution during multiple compressions in a channel die [22]. As mentioned above, there are experimental evidences about the occurrence of texture weakening during some SPD processes, which are similar to multiple compressions in a channel die [10, 11, 13-15], but to the authors' knowledge, the reason of this texture weakening has not been explained. In the current work, texture evolution during multiple compressions in a channel die of commercially pure copper is studied and a procedure for interpreting the cause of texture weakening during this type of SPD process, based on the conservation of ODF in the Euler angle space is proposed. This is novel, and to the authors' knowledge, has not been reported so far.

2. Experimental Procedure

The as-received material was a billet of commercially pure copper from which samples with dimensions of 7.5 mm×14.8 mm×15 mm were cut by wire electro-discharge machining and used for subsequent processing. These specimens were fully annealed at 873K for 4 h to eliminate the effects of previous thermomechanical history.

The annealed samples were compressed repetitively in a channel die at room temperature and with a ram speed of 25 mm/s. Fig. 1 shows the deformation scheme during multiple compressions in a channel die. The sides of the specimen are designated as A, B, and C. The first pass of the process has been carried out on face A. During this pass, a 15 mm high specimen with 14.8 mm×7.5 mm cross-section was placed in the die and

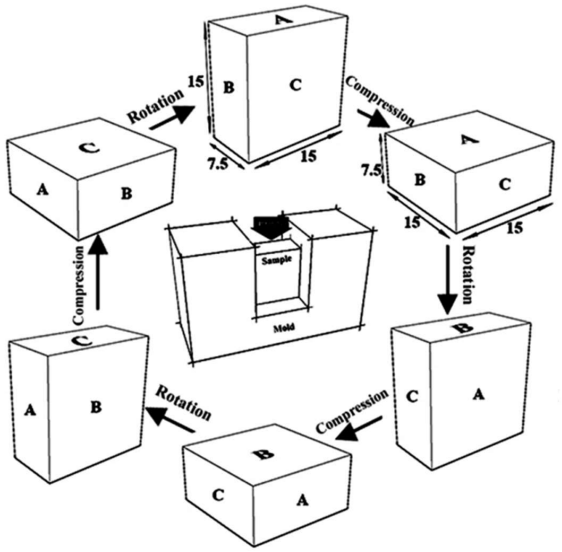

Fig. 1. Deformation scheme during multiple compressions in a channel die.

compressed to half of its height. It is worth noting that the specimen located in the die so that the 14.8 mm side just slides into the 15 mm wide channel at the end of the pass. After the first pass, the specimen was rotated so that the 15 mm width of the processed specimen in the first pass of pressing becomes the height of the sample during the second pass and the 14.8 mm side slides into the width of the channel, the same as the previous pass. Again, the sample was compressed to half of its height. The aforementioned stages repeated, and the third pass of the process was carried out on face C. This sequence ensures that the specimen is deformed in three mutually perpendicular directions. It needs to be mentioned that after each pass of the process, the bulged portion of the sample was grinded to preserve initial dimensions. The above-mentioned stages were repeated up to six passes ($\varepsilon_{eq} = 4.8$). Textures of annealed and processed samples after 2, 4, and 6 passes were measured by X-ray diffraction. Three incomplete pole figures, i.e. (111), (200), and (220) were measured at the center of the specimens using the Schultz back-reflection method on a Rigaku Ultima IV goniometer with a copper tube and monochromator. After theoretical defocussing and background correction of the raw data, corrected pole figures were obtained. Then the ODF was calculated from these pole figures using the MATLAB MTEX toolbox [23]. Based on the mean RP errors between experimental and calculated pole figures, having halfwidth values between 4 and 32 degrees, and considering 100 iterations, the optimum value of halfwidth for all ODF calculations was determined to be equal to 7 degrees.

Microhardness of the multiple compressed samples in a channel die was measured on the polished specimens by a Buhler microhardness testing machine using Vickers indenter and under an applied load of 500 gr. The mean value of 4 separate hardness values measured at random places of the specimen's surface was considered as the microhardness of the annealed and severely deformed samples.

The annealed specimen was polished then etched by a solution containing 10 g of $FeCl_3$, 5 ml HCl and 100 ml ethanol. The microstructure of the prepared sample by the aforementioned procedure was studied by an optical microscope. The severely deformed specimens were electropolished by the use of Struers D2 electrolyte (500 ml of distilled water, 250 ml phosphoric acid, 250 ml propanol, and 5 g urea) for 20 seconds with 24 v. The microstructure of these specimens was studied by LEO 1450 VP scanning electron microscope (SEM) using electron channeling contrast imaging (ECCI) method.

Microhardness measurements and microstructural study were carried out on the surface perpendicular to compression direction at each specific pass of the process. Moreover, the compression direction was considered as ND, flow direction assumed as RD, and the constraint direction designated as TD for reporting the texture at each specific pass of multiple compressions in a channel die.

3. Continuity Equation in the Crystal Orientation (Euler Angle) Space

The continuity equation of the ODF in the crystal orientation space can be used to estimate texture evolution during the deformation process [19]. The method of derivation of this equation and its closed form solution is described in brief; for the sake of completeness. It is worth to be noted that although the

principle of conservation has been used for predicting the variation of ODF; to the authors' knowledge, the closed form solution of the partial differential equation which is obtained as a result of the application of the conservation principle, has not been reported up to this time.

The normalization condition of orientation distribution function, f(g) is

$$\frac{1}{8\pi^2}\int_{\phi_1}\int_{\phi}\int_{\phi_2} f(g)dg = 1 \tag{1}$$

where (ϕ_1, ϕ, ϕ_2) are the three Euler angles (Bunge definition) and dg can be expressed as follows

$$\mathrm{d}g = \sin\phi \, d\phi_1 d\phi d\phi_2 \tag{2}$$

The Euler angles can be regarded as coordinates in three-dimensional curved Riemannian space of orientation. Thus, considering (ϕ_1, ϕ, ϕ_2) as contra variant coordinates, the metric tensor is obtained as:

$$[G] = \begin{bmatrix} 1 & 0 & \cos\phi \\ 0 & 1 & 0 \\ \cos\phi & 0 & 1 \end{bmatrix} \tag{3}$$

The determinant of $[G]$, i.e. $|G|$ equals to $\sin^2\phi$. Therefore, based on Riemannian geometry, the volume element of the orientation space can be written as [24]:

$$dv = \sqrt{|G|}d\phi_1 d\phi d\phi_2 = \sin\phi \, d\phi_1 d\phi d\phi_2 \tag{4}$$

Considering f(g) as the volume fraction of grains whose lattice orientations are located in the element dg, for a given g, the increase of the quantity of grains in volume v with respect to time can be written as:

$$\frac{\partial}{\partial t}\iiint_g f(g)\, dg \tag{5}$$

The quantity of grains moving across nds and leaves the element ds can be expressed by the following equation:

$$\oint_s f(g).R.nds \tag{6}$$

where $R = (\dot{\phi}_1, \dot{\phi}, \dot{\phi}_2)$, ds, and n are rotation velocity, element of surface in Euler angle space and outward unit vector, normal to the surface element, respectively.

Considering Eq. (1), the change of the quantity of grains in volume v with respect to time, i.e. Eq. (2), plus the quantity of grains moving across nds should be equal to zero, or:

$$\frac{\partial}{\partial t}\iiint f(g)dg = -\oint_s f(g).Rnds \tag{7}$$

Taking the determinant of metric tensor into consideration and using divergence theorem, the following equation obtains:

$$\begin{aligned}\frac{\partial}{\partial t}\iiint f(g)\sin\phi \, d\phi_1 d\phi d\phi_2 \\ = -\iiint \frac{1}{\sin\phi}\{\nabla.[f(g)\sin\phi\,.R]\} \\ \sin\phi \, d\phi_1 d\phi d\phi_2\end{aligned} \tag{8}$$

It is worth noting that divergence of f.R in the orientation space is defined as:

$$\begin{aligned}\mathrm{div}(f.R) &= \frac{1}{\sin\phi}(\nabla.(f(g)\sin\phi\,.R) \\ &= \frac{1}{\sin\phi}\left[\frac{\partial(\sin\phi\, f(g)\dot{\phi}_1}{\partial\phi_1}\right. \\ &\quad + \frac{\partial(\sin\phi\, f(g)\dot{\phi}}{\partial\phi} \\ &\quad \left. + \frac{\partial(\sin\phi\, f(g)\dot{\phi}_2}{\partial\phi_2}\right]\end{aligned} \tag{9}$$

Eq. (8) leads to the following equation:

$$\frac{\partial f}{\partial t} = -\frac{1}{\sin\phi}\nabla.[f(g)\sin\phi\,.R] \tag{10}$$

Eq. (10) is the continuity equation for f(g) in the orientation space. Eq. (10) can be rewritten in the following form:

$$\frac{\partial f}{\partial t} = -\frac{1}{\sin\phi}[f]\sin\phi \left[\frac{\partial \dot{\phi}_1}{\partial \phi_1} + \frac{\partial \dot{\phi}}{\partial \phi} + \frac{\partial \dot{\phi}_2}{\partial \phi_2}\right] - \left(\dot{\phi}_1 \frac{\partial f}{\partial \phi_1} + \dot{\phi} \frac{\partial f}{\partial \phi} + \dot{\phi}_2 \frac{\partial f}{\partial \phi_2}\right) - f\dot{\phi}\cot\phi \quad (11)$$

Simplifying Eq. (11) leads to:

$$\frac{\partial \ln f}{\partial t} + \dot{\phi}_1 \frac{\partial \ln f}{\partial \phi_1} + \dot{\phi} \frac{\partial \ln f}{\partial \phi} + \dot{\phi}_2 \frac{\partial \ln f}{\partial \phi_2} = -\left[\frac{\partial \dot{\phi}_1}{\partial \phi_1} + \frac{\partial \dot{\phi}}{\partial \phi} + \frac{\partial \dot{\phi}_2}{\partial \phi_2}\right] - \dot{\phi}\cot\phi \quad (12)$$

Applying the method of characteristics for solving Eq. (12), the following equations obtain:

$$dt = \frac{d\phi_1}{\dot{\phi}_1} = \frac{d\phi}{\dot{\phi}} = \frac{d\phi_2}{\dot{\phi}_2} = \frac{d\ln f}{-\left[\frac{\partial \dot{\phi}_1}{\partial \phi_1} + \frac{\partial \dot{\phi}}{\partial \phi} + \frac{\partial \dot{\phi}_2}{\partial \phi_2}\right] - \dot{\phi}\cot\phi} \quad (13)$$

Solving equations (13) simultaneously, the following relations are obtained:

$$\ln f = \int \left[-\left[\frac{\partial \dot{\phi}_1}{\partial \phi_1} + \frac{\partial \dot{\phi}}{\partial \phi} + \frac{\partial \dot{\phi}_2}{\partial \phi_2}\right] - \dot{\phi}\cot\phi\right] dt \quad (14)$$

$$\phi_1 = \int \dot{\phi}_1 \mathrm{d}t + (\phi_1)_0 \quad (15)$$

$$\phi = \int \dot{\phi} \mathrm{d}t + (\phi)_0 \quad (16)$$

$$\phi_2 = \int \dot{\phi}_2 \mathrm{d}t + (\phi_2)_0 \quad (17)$$

Considering the value of f at the start of time integration as $f((\phi_1)_0, (\phi)_0, (\phi_2)_0)$, the closed form solution of Eq. (12) can be stated as:

$$f(\phi_1, \phi, \phi_2) = f((\phi_1)_0, (\phi)_0, (\phi_2)_0) \exp\left\{\int \left[-\left[\frac{\partial \dot{\phi}_1}{\partial \phi_1} + \frac{\partial \dot{\phi}}{\partial \phi} + \frac{\partial \dot{\phi}_2}{\partial \phi_2}\right] - \dot{\phi}\cot\phi\right] dt\right\} \quad (18)$$

where ϕ_1, ϕ, and ϕ_2 are obtained by equations (15)-(17). The rotation velocity, R and its divergence for each deformation process are independent of initial texture and strain. Therefore, it can be said that the aforementioned parameters are solely related to the deformation processes and for each specific deformation process, the same function for R and its divergence can be used, regardless of the strain and initial texture [17, 20].

4. Results and Discussion

Fig. 2 shows the texture of fully annealed specimens as the ϕ_2-constant ODF sections. From this figure, it is clear that the main texture components of this sample are Cube $(\phi_1 = 0°, \phi = 0°, \phi_2 = 0°)$, Brass $(\phi_1 = 35°, \phi = 45°, \phi_2 = 0°)$ and Goss $(\phi_1 = 0°, \phi = 45°, \phi_2 = 0°)$ orientations. A prominent rotation of Cube texture around transverse direction (TD) is observable at $(\phi_1 = 90°, \phi = 0 - 45°, \phi_2 = 0°)$. The Cube, Cube TD and Goss orientations are texture components usually observed in recrystallized FCC metals, while Brass orientation is a deformation component in FCC metals and is probably a partial remnant of deformation texture which has been formed due to previous deformation on the as-received material [25]. Based on the values of ODF, it can be said that the overall texture of annealed specimen is weak.

Texture of the multiple compressed samples have been shown in Fig. 3(a)-(c) as the ϕ_2 constant ODF sections after two, four and six passes. Based on Fig. 3(a), it can be said that in the samples subjected to two passes of multiple compressions in a channel die, Cube, Goss and Bs2 orientations are observable and Cube orientations experience no change in intensity in comparison with that of annealed specimen while the intensity of Goss and Bs2 decreases and increases, respectively. Moreover, Bs2 component spreads along RGoss $(\phi_1 = 45°, \phi = 0/90°, \phi_2 = 0°)$ and between Goss and Bs2 along Beta fiber. Fig. 3(b) shows that after four passes of the process, the region corresponding to Goss orientation shrinks and the Beta fiber divides into two parts and the orientation at $(\phi_1 = 45°, \phi = 0°, \phi_2 = 0°)$ displaces to Bs2 and then moves to reach $(\phi_1 = 45°, \phi = 90°, \phi_2 = 0°)$ orientation. The position of the Cube component is the same as those of the annealed and two pass processed samples. The Beta fiber in the sample processed by four passes of the process is

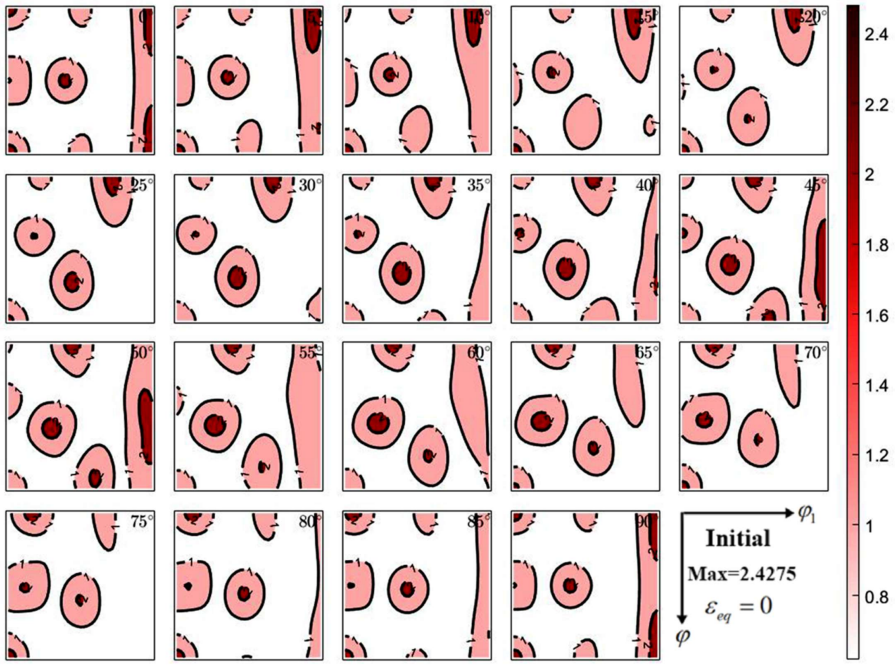

Fig. 2. The texture of fully annealed specimens as the ϕ_2-constant ODF sections.

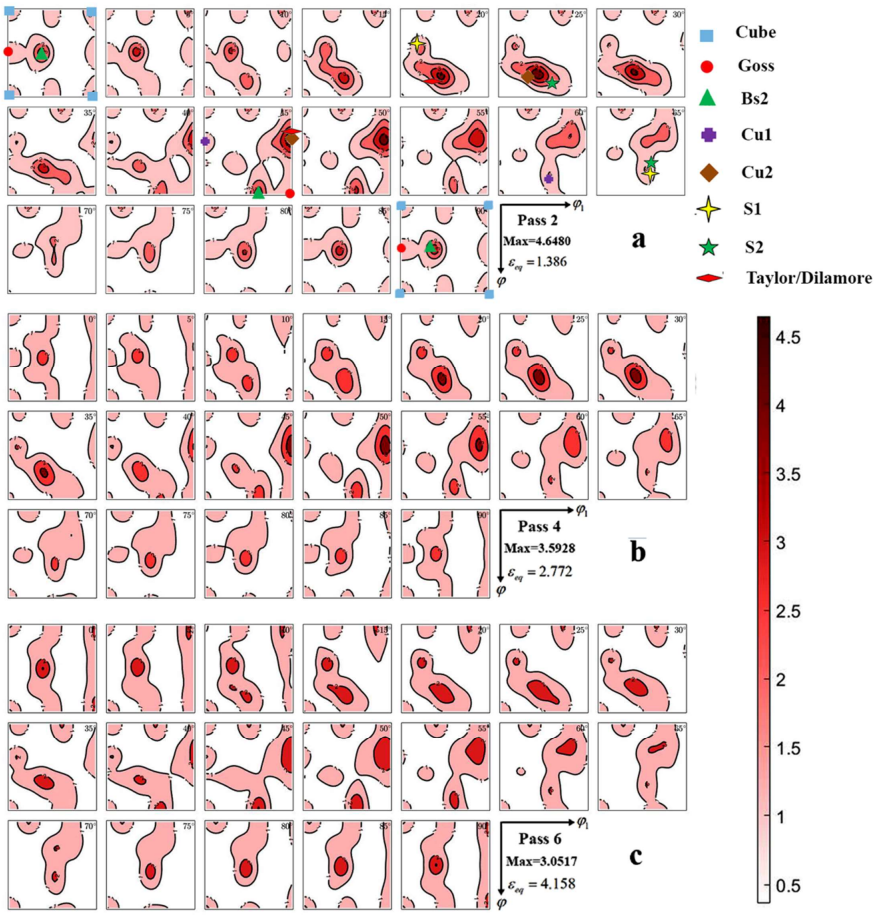

Fig. 3. Texture of the multiple compressed samples after a) two, b) four, and c) six passes.

wider than that of specimen subjected to two passes of multiple compressions in a channel die. Texture of specimen subjected to six passes of multiple compressions in channel die has been shown in Fig. 3(c). It is clear from this figure that Goss orientation has disappeared completely; the width of the fiber running from Bs2 to RGoss increased in comparison with that of specimen subjected to four passes of the process and overall texture of the six-pass processed sample weakened.

Fig. 4 shows the microhardness changes together with the evolution of the microstructure of the samples subjected to even passes of multiple compressions in a channel die. Based on this figure, it can be said that there is a considerable increase of microhardness after two passes of the process while in subsequent passes the microhardness remains almost constant. From the micrographs, it is clear that the grain size of the samples changes from approximately 11 µm to about 0.36 µm after two passes of the process and reductions of average grain size continues during the subsequent passes and it can be said that the multiple compressions in a channel die are capable of producing ultra-fine grain materials. The average grain size of processed specimens after four and six passes are 0.34 µm and 0.25 µm, respectively. From Fig. 4, it is clear that grain size reduction of the studied material mostly occurs after the second pass of the process and at the subsequent passes, the rate of grain size reduction decreases appreciably. This phenomenon is consistent with that of other SPD processes [1, 2]. Therefore, the microstructure of the processed specimens after 2, 4, and 6 passes are similar, which is consistent

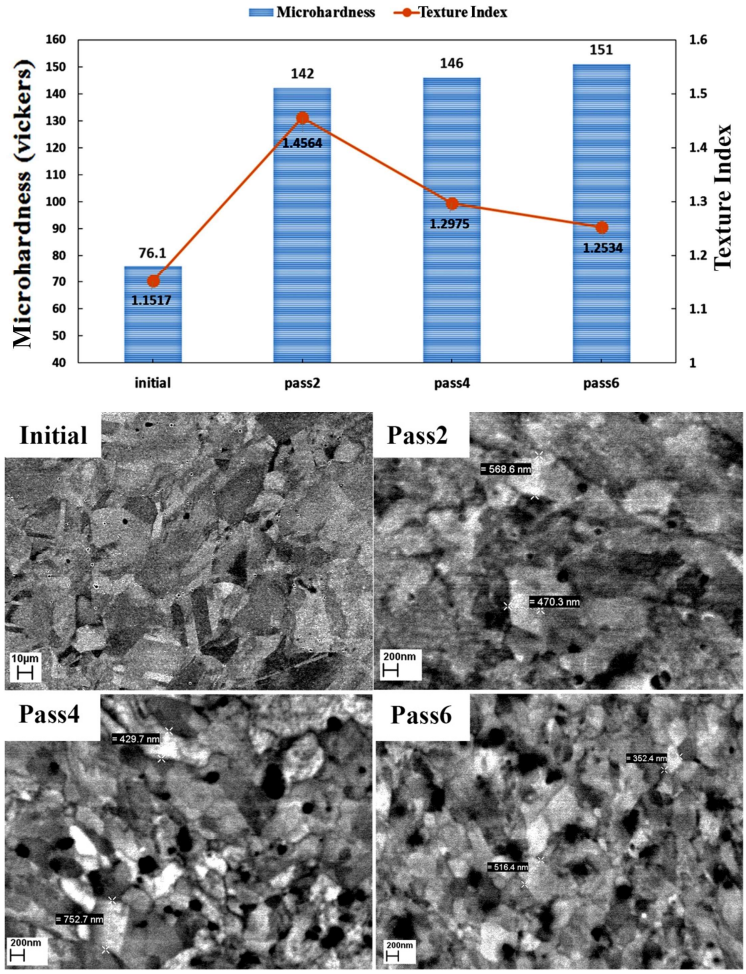

Fig. 4. The microhardness and texture index changes together with the evolution of microstructure of the processed samples.

with microhardness measurements.

A texture component is called stable when the rotation speed vanishes, i.e. $(\dot{\phi}_1, \dot{\phi}, \dot{\phi}_2) = (0,0,0)$ and the neighboring orientations tend to move towards this texture component. This tendency can be expressed as [17, 21]:

$$\frac{\partial \dot{\phi}_1}{\partial \phi_1} + \frac{\partial \dot{\phi}}{\partial \phi} + \frac{\partial \dot{\phi}_2}{\partial \phi_2} \langle 0 \qquad (19)$$

Considering Eq. (18), it is evident that for a stable texture component, the value of ODF increases during deformation. Therefore, the above-mentioned definition of a stable texture component is rational. The rotation fields for some ideal orientations usually observe in rolling texture of FCC metals have been calculated; assuming Taylor like visco-plastic model and tabulated in Table 1.

Based on the definition of stable texture components mentioned above and Table 1, it can be said that all of the tabulated ideal orientations are stable; except copper texture components which is metastable, because $\dot{\phi}$ does not vanish for this component; therefore, its location changes in Euler angle space during deformation. It is noteworthy that based on the values of $(\dot{\phi}_1, \dot{\phi}, \dot{\phi}_2)$, the copper component of texture slowly displaces in Euler angle space. Moreover, during deformation, the ODF increases since $\frac{\partial \dot{\phi}_1}{\partial \phi_1} + \frac{\partial \dot{\phi}}{\partial \phi} + \frac{\partial \dot{\phi}_2}{\partial \phi_2} + \dot{\phi} \cot \phi$ is almost less than zero for this texture component, during its course in Euler angle space as a result of deformation.

Plane strain mode of deformation in multiple compressions in a channel die is similar to that of rolling process. Therefore, it seems that changing the strain direction in this process affects the texture evolution like that occurs in cross rolling. As mentioned before in multiple compressions in a channel die after each pass, the specimen is rotated by 90° around two mutually perpendicular directions. Supposing plane strain compression analogous to rolling, these perpendicular directions, are considered as rolling and normal directions, respectively (RD and ND). Formation of Alpha and Beta fibers during rolling deformation of pure FCC metals with medium to high SFE has been proven experimentally [25]. The Alpha fiber initiates at Goss orientation and extends to the Brass. The Beta fiber is considered as an orientation tube, running from Copper orientation through S orientation to the Brass where it meets the Alpha fiber. Development of Alpha and Beta fibers during plane strain compression can be interpreted successfully by the use of stability analysis and considering Table 1. Since during deformation, all orientations in Euler angle space move towards stable orientations. Therefore, it is anticipated that ODF of stable components of orientations increase or at least remain constant while ODF of other orientations decrease. Taking Eq. (18) into consideration, it can be said

Table 1. Rotation field for some ideal orientations appear in rolling texture of FCC metals [26]

Component / Parameter	Cube	Goss	Copper	Brass	Taylor
$\dot{\phi}_1$	0	0	0	0	0
$\dot{\phi}$	0	0	-0.47	0	0
$\dot{\phi}_2$	0	0	0	0	0
$\frac{\partial \dot{\phi}_1}{\partial \phi_1}$	-1	1	1	-1.01	1
$\frac{\partial \dot{\phi}}{\partial \phi}$	1	-1	-3.3	-0.67	-3.47
$\frac{\partial \dot{\phi}_2}{\partial \phi_2}$	0	-6	-3.65	-2.43	-4.46
$\sum \frac{\partial \dot{\phi}_1}{\partial \phi_1}$	0	-6	-5.97	-4.11	-6.93
$\dot{\phi} \cot \phi$	0	0	-0.67	0	0
$\operatorname{div} \dot{g}$	0	-6	-6.64	-4.11	-6.93

that the value of $\int \left[\frac{\partial \dot{\phi}_1}{\partial \phi_1} + \frac{\partial \dot{\phi}}{\partial \phi} + \frac{\partial \dot{\phi}_2}{\partial \phi_2} + \dot{\phi}\cot\phi\right] dt$ is less than zero for Alpha and Beta fibers and thus, the ODF of these fibers increases, while for other orientations, the value of the aforementioned quantity is greater than zero and the ODF decreases in orientations which do not coincide with Alpha and Beta fibers.

It is clear from Fig. 1 that rotation of the specimen after each pass of multiple compressions in a channel die causes to change from normal direction into rolling direction and transverse direction into normal direction, respectively. Therefore, the position of main components of plane strain compression at the start of multiple compressions in a channel die's even passes can be determined, considering ND to RD and TD to ND interchanges and the main texture components of one pass of the process as follows: Cu1 or $\{112\}\langle 110\rangle$ locating at $(0°, 35°, 45°)$ in the orientations space changes into $\{111\}\langle 112\rangle$ or $(30°, 54°, 45°)$ in the orientation space. Cu2 or $\{112\}\langle 111\rangle$ which is located at $(90°, 35°, 45°)$ in orientation space transforms into $\{011\}\langle 211\rangle$ or $(35°, 45°, 0°)$ in the orientation space which is Bs2 component. S1 or $\{123\}\langle 9125\rangle$ located at $(32°, 35°, 25°)$ in the orientation space displaces into $\{111523\}\langle 123\rangle$ or $(25°, 39°, 36°)$ in the orientation space. S2 or $\{123\}\langle 475\rangle$which is at $(61°, 35°, 65°)$ in the orientation space changes into $\{9811\}\langle 123\rangle$ or $(25°, 47°, 48°)$ at the orientation space. Bs1 or $\{011\}\langle 111\rangle$ located at $(55°, 45°, 0°)$in the orientation space transforms into $\{111\}\langle 112\rangle$or Cu1 orientation and Bs2 or $\{011\}\langle 211\rangle$displaces into $\{111\}\langle 110\rangle$ or $(60°, 55°, 45°)$ in the orientation space. The Cube or $\{001\}\langle 100\rangle$ texture component, which is at $(0°, 0°, 0°)$ transforms into crystallographically equivalent orientation. As mentioned before, Cube, Goss, and Bs2 components are the main observable texture components in multiple compressed specimens in a channel die after even passes. Taking a look at Table 1, it is clear that Copper and Brass components are stable/metastable texture components in rolling of FCC metals with medium to high SFE. Therefore, the existence of Cu1 and Bs2 in the even pass processed specimens is anticipated. It is worth to be noted that the Cu2 component of odd pass processed specimens transforms into Bs2, and Bs1 component of the odd pass processed samples changes into Cu1 component at the start of even passes. Thus, it can be said that ODF values of Cu1 and Bs2 components increase at the end of even passes of multiple compressions in a channel die. The other stable/metastable texture components of the odd processed specimens change into orientations which are note stable/metastable (Table 1 and Eq. (18)) at the start of even passes, thus, these components rotate towards more stable orientations during even passes of the process and are not visible in the texture of specimens subjected to even passes of multiple compressions in a channel die. Cube component of the texture experiences no change during plane strain compression. This phenomenon can be estimated using Table 1. According to this table and taking Eq. (18) into consideration, the value of ODF for Cube component and its position in the orientation space should remain constant during plane strain compression. Based on the aforementioned discussion, Cube component of texture at the end of odd passes of multiple compressions in a channel die transforms into Cube component at the start of even passes of the process, thus, the ODF value of the Cube component should remain constant in the texture of specimen subjected to even passes of the process. Variation of ODF values along Alpha and Beta fibers has been illustrated in Fig. 5(a) and 5(b). From this figure, it is clear that the ODF values of Cu1 and Bs2 components of texture increase, Goss component of texture disappears (ODF value is less than that of random texture) and ODF value of Cube component remain almost constant after even passes of multiple compressions in a channel die; which correlates well with predictions made by the use of Table 1 and Eq. (18). From the above-mentioned discussion, it is clear that the ODF values decrease except at Cu1 and Bs2 positions in which the value of ODF increases and ODF of cube orientation remains constant. Defining the texture index, a single parameter that characterizes texture sharpness, as $\oint [f(g)]^2 dg$ [27], it can be said that after even passes of multiple compressions in a channel die, texture index decreases or texture weakens. The values of texture index at even passes of multiple compressions in a channel die have been superimposed on Fig. 4.

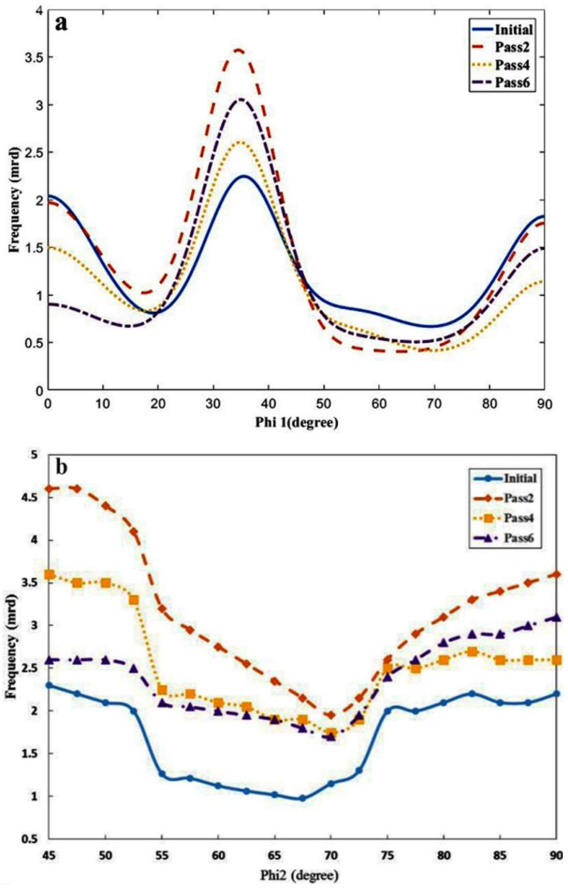

Fig. 5. Variation of ODF values along a) Alpha, and b) Beta fibers.

5. Conclusion

Texture evolution of the fully annealed commercially pure copper was studied after two, four, and six passes of multiple compressions in a channel die and it was found that this process caused texture weakening in this material. An analytical equation for ODF values of the processed sample during each pass of compression was obtained. In this equation the ODF is calculated as a function of the initial ODF of the sample and crystallographic rotation speed in Euler angle space. Based on this equation, the location of stable components and evolution of texture were estimated for the specimens subjected to even passes of multiple compressions in channel die. Comparing the estimation of texture evolution by the use of the analytical equation with those measured experimentally showed that there is a reasonable agreement between estimations and experimental results.

6. References

[1] E. Bagherpour, N. Pardis, M. Reihanian, and R. Ebrahimi, An overview on severe plastic deformation: research status, techniques classification, microstructure evolution, and applications, *The International Journal of Advanced Manufacturing Technology*, 100(5-8) (2019) 1647-1694.

[2] Y. Estrin, A. Vinogradov, Extreme grain refinement by severe plastic deformation: A wealth of challenging science. *Acta Materialia*, 61(3) (2013) 782-817.

[3] R.Z. Valiev, R.K. Islamgaliev, I.V. Alexandrov, Bulk nanostructured materials from severe plastic deformation, *Progress in Materials Science*, 45(2) (2000) 103-189.

[4] R.Z. Valiev, N.A. Krasilnikov, N.K. Tsenev, Plastic deformation of alloys with submicron-grained structure, *Materials Science and Engineering: A*, 137 (191) 35-40.

[5] E. Bagherpour, M. Reihanian, N. Pardis, R. Ebrahimi, T.G. Langdon, Ten years of severe plastic deformation (SPD) in Iran, part I: equal channel angular pressing (ECAP), *Iranian Journal of Materials Forming*, **5**(1) (2018) 71-113.

[6] Y. Saito, H. Utsunomiya, N. Tsuji, T. Sakai, Novel ultra-high straining process for bulk materials-development of the accumulative roll-bonding (ARB) process, 47(2) (1999) 579-583.

[7] G. Salishchev, R. Zaripova, R. Galeev, O. Valiakhmetov, Nanocrystalline structure formation during severe plastic deformation in metals and their deformation behaviour, *Nanostructured Materials*, 6(5-8) (1995) 913-916.

[8] J. Richert, M. Richert, A new method for unlimited deformation of metals and alloys, *Aluminium*, 62 (1986) 604-607.

[9] A. Kundu, R. Kapoor, R. Tewari, J.K. Chakravartty, Severe plastic deformation of copper using multiple compression in a channel die, *Scripta Materialia*, 58(3) (2008) 235-238.

[10] S. Biswas, S. Suwas, Evolution of sub-micron grain size and weak texture in magnesium alloy Mg–3Al–0.4Mn by a modified multi-axial forging process, *Scripta Materialia*, 66(2) (2012) 89-92.

[11] Q. Chen, D. Shu, C. Hu, Z. Zhao, B. Yuan, Grain refinement in an as-cast AZ61 magnesium alloy processed by multi-axial forging under the multitemperature processing procedure, *Materials Science and Engineering: A*, 541 (2012) 98-104.

[12] X.S. Xia, C. Ming, F.Y. Fan, C.H. Zhu, J. Huang, T.Q. Deng, S.F. Zhu, Microstructure and mechanical properties of isothermal multi-axial forging formed

AZ61 Mg alloy, *Transactions of Nonferrous Metals Society of China*, 23(11) (2013) 3186-3192.

[13] K. Li, V.S.Y. Injeti, P. Trivedi, L.E. Murr, R.D.K. Misra, Nanoscale deformation of multiaxially forged ultrafine-grained Mg-2Zn-2Gd alloy with high strength-high ductility combination and comparison with the coarse-grained counterpart, *Journal of Materials Science & Technology*, 34(2) (2018) 311-316.

[14] S. Ringeval, D. Piot, C. Desrayaud, J.H. Driver, Texture and microtexture development in an Al–3Mg–Sc(Zr) alloy deformed by triaxial forging, *Acta Materialia*, 54(11) (2006) 3095-3105.

[15] A.K. Padap, G.P. Chaudhari, V. Pancholi, S.K. Nath, Warm multiaxial forging of AISI 1016 steel, *Materials & Design*, 31(8) (2010) 3816-3824.

[16] A.K. Padap, A.P. Yadav, P. Kumar, N. Kumar, Effect of aging heat treatment and uniaxial compression on thermal behavior of 7075 aluminum alloy, *Materials Today: Proceedings*, 33 (2020) 5442-5447.

[17] A. Clement, Prediction of deformation texture using a physical principle of conservatiol, *Materials Science and Engineering*, 55(2) (1982) 203-210.

[18] K. Wierzbanowski, A. Clement, Rotation field and continuity equation for texture evolution, *Crystal Research and Technology*, 19(2) (1984) 201-212.

[19] Y. Zhou, L.S. Tóth, K.W. Neale, On the stability of the ideal orientations of rolling textures for FCC polycrystals, *Acta Metallurgica et Materialia*, 40(11) (1992) 3179-3193.

[20] L.S. Tóth, J.J. Jonas, D. Daniel, R.K. Ray, Development of ferrite rolling textures in low- and extra low-carbon steels, *Metallurgical Transactions A*, 21(11) (1990) 2985-3000.

[21] L.S. Tóth, B. Beausir, D. Orlov, R. Lapovok, A. Haldar, Analysis of texture and R value variations in asymmetric rolling of IF steel, *Journal of Materials Processing Technology*, 212(2) (2012) 509-515.

[22] S. Kandalam, R.K. Sabat, N. Bibhanshu, G.S. Avadhani, S. Kumar, S. Suwas, Superplasticity in high temperature magnesium alloy WE43, *Materials Science and Engineering: A*, 687 (2017) 85-92.

[23] D. Mainprice, F. Bachmann, R. Hielscher, H. Schaeben, Descriptive tools for the analysis of texture projects with large datasets using MTEX: strength, symmetry and component, *Geological Society, London, Special Publications*, 409(1) (2015) 251-271.

[24] P.H. Dluzewski, Crystal orientation spaces and remarks on the modelling of polycrystal anisotropy, *Journal of the Mechanics and Physics of Solids*, **39**(5) (1991) 651-661.

[25] O. Engler, V. Randle, Introduction to texture analysis: macrotexture, microtexture, and orientation mapping, Second edition, CRC Press, 2009.

[26] S. Ahmadi, A new Eulerian-based double continuity model for predicting the evolution of pair correlation statistics under large plastic deformations, Bringham Young University, 2010.

[27] H.J. Bunge, Texture analysis in materials science: mathematical methods, Butterworth, 1982.